ELSEVIER

Physics of the Earth and Planetary Interiors 124 (2001) 71–79

PHYSICS OF THE EARTH AND PLANETARY INTERIORS

www.elsevier.com/locate/pepi

Anomalous compression and equation of state of coesite

R.J. Angel*, J.L. Mosenfelder[1], C.S.J. Shaw[2]

Bayerisches Geoinstitut, Universität Bayreuth, D-95440 Bayreuth, Germany

Received 1 February 2001; accepted 1 February 2001

Abstract

The compressional behaviour of coesite has been determined to a maximum pressure of 9.6 GPa by room-temperature single-crystal X-ray diffraction measurements on three crystals selected from two different synthetic samples. There is no evidence for any phase transitions in this pressure range. The new direct measurements show that coesite is approximately 1% denser at 9–10 GPa (at room temperature) than predicted by extrapolation of the previously reported EoS. The volume-pressure data of all three samples cannot be adequately described by any available third-order equation of state. Refined parameters for a fourth-order Birch-Murnaghan EoS are $K_{T0} = 100.8 \pm 0.5$ GPa, $K'_{T0} = 1.8 \pm 0.3$ and $K''_{T0} = 0.57 \pm 0.06\,\text{GPa}^{-1}$. The anomalous positive value of K''_{T0} appears to be related to the anomalous compression of the *c*-axis of the structure that exhibits an initial softening with increasing pressure. At pressures in excess of 8 GPa the bulk modulus of coesite is some 20 GPa less than that previously predicted, and the impedence contrast between coesite and stishovite is therefore some 10% greater than would have been estimated on the basis of the previous EoS parameters.

Keywords: Coesite; Equation of state; Elasticity; Bulk modulus

1. Introduction

Coesite is a polymorph of silica, only stable at pressures in excess ~2.5 GPa at 500°C. At lower pressures it is thermodynamically unstable with respect to quartz. Before 1977, coesite was only known from meteorite impact craters, in which it was formed from quartz during high-pressures and temperatures generated by the impact and then quenched sufficiently rapidly to prevent reversion to quartz. More recently, preserved coesite has been found in deeply subducted crustal rocks in collision belts (e.g. Chopin, 1983; Parkinson and Katayama, 1999; Parkinson, 2000). Such occurrences provide definitive proof that the rocks in which it occurs have experienced depths of at least 100 km and have been subsequently exhumed under conditions that prevent the inversion to quartz. Coesite can also be readily synthesised from quartz in the laboratory between pressures of 3 and 9 GPa at high temperatures; indeed the inversion between quartz and coesite is used as a standard calibration of pressure in piston-cylinder apparatus. The inversion of coesite at higher pressures to stishovite is used to calibrate multi-anvil presses in the 10 GPa pressure range. This transformation has also recently been proposed by Williams and Revanaugh (2000) as a possible alternative explanation to the

* Corresponding author. Present address: Crystallography Laboratory, Department of Geological Sciences, Virginia Polytechnic and State University, Blacksburg, VA 24061-0420, USA.
Tel.: +1-540-231-7974; fax: +1-540-231-3386.
E-mail address: rangel@vt.edu (R.J. Angel).
[1] Department of Geological and Planetary Sciences, California Institute of Technology, M/C 170-25, Pasadena, CA 91125, USA.
[2] Mineralogisch-Petrologisches-Institut, Georg-August-Universität, Goldschmidtstr. 1, D-37077, Göttingen, Germany.

0031-9201/01/$ – see front matter
PII: S0031-9201(01)00184-4

orthopyroxene-clinopyroxene inversion (Woodland and Angel, 1997) for the enigmatic "X" seismic discontinuity within the upper mantle.

A knowledge of the elastic properties of coesite is therefore essential for three reasons. Preservation of coesite in high-pressure rocks is dependent upon the exclusion of fluid which catalyses the inversion to quartz; this only occurs if the matrix of other minerals around the coesite remains unbroken. This in turn is determined by the elastic properties of the coesite and the matrix as well as their breaking strengths (Gillet et al., 1984; van der Molen and van Roermond, 1986). Secondly, the compressional elastic constants are a derivative of volume with respect to pressure, so measurement of the elasticity and/or volume of coesite is necessary for more precise calculation of the positions in P–T space of the equilibrium phase boundaries between coesite and the other silica polymorphs. Thirdly, the seismic velocity jump associated with these transitions, of which the coesite-stishovite transformation is potentially the more important, is determined by the elastic properties of the two phases.

Unfortunately, values of some of the thermodynamic properties of coesite appear to be anomalous, and much of the available experimental data for coesite is inconsistent. For example, both the thermal expansion and the elastic modulus tensor indicate that the response of the coesite structure is extremely anisotropic, while the volume thermal expansion coefficient $\alpha_V = 6 \times 10^{-6}\,K^{-1}$ at room conditions is extremely small (Galkin et al., 1987). This value, coupled with measurements of the heat capacity (Hemingway et al., 1998) and the adiabatic bulk modulus (Weidner and Carleton, 1977), implies a value of ~0.32 for the Gruneisen ratio γ. But this is only one-half of the value deduced from the pressure dependence of the observed Raman and infra-red bands (Hemley, 1987; Williams et al., 1993). Even the larger spectroscopic value of γ leads to a value, at 300 K, of 1.012 for the factor $(1 + \alpha_V \gamma T)$ which is thermodynamically identical to the ratio of the adiabatic (K_{S0}) to isothermal (K_{T0}) bulk moduli. However, the experimentally determined values of these two moduli (Weidner and Carleton, 1977; Levien and Prewitt, 1981) yield $K_{S0}/K_{T0} = 1.14 \pm 0.07$. Furthermore, the single-crystal compression data used to obtain K_{T0} yielded an abnormally high value of $K'_{T0} = (dK_T/dP)_{P=0} = 8.4 \pm 1.9$ (Levien and Prewitt, 1981), especially considering that coesite has strong structural similarities to the feldspars, which have values ranging from $K'_{T0} \sim 3$ for plagioclases (Angel, 1996) to $K'_{T0} \sim 5$ for albite (Downs et al., 1994). We have therefore undertaken a single-crystal compression study of coesite to a maximum pressure of ~9.6 GPa with the aim of re-determining its isothermal EoS and thereby contributing to a resolution of these discrepancies.

2. Experimental

Coesite single crystals were synthesised in two separate experiments. Run CS45 was performed in a piston cylinder apparatus at a nominal (uncorrected) pressure of 3.15 GPa and 700°C for 68 h using a NaCl-pyrex cell assembly (Shaw, 1999). The powdered natural quartz and water starting materials were contained in a gold capsule. The synthesis of the U1686 sample was performed at 7 GPa and 1200°C in a multi-anvil apparatus. The starting assemblage was silica glass and synthetic talc (to provide a source of water) loaded into a Pt capsule along with a layer of a Ni + NiO oxide powder in order to buffer the oxygen fugacity. Full details are provided in Mosenfelder (2000). The water-saturated conditions of both runs resulted in the synthesis of large (>100 μm) single crystals of coesite. The hydrogen content of the coesite from U1686 was measured as ~730 ppm H/Si, equivalent to 110 ppm H_2O by weight (Mosenfelder, 2000). The hydrogen content of the CS45 sample was not measured, but is expected to be lower than in U1686 because of the pressure dependence of H solubility in coesite (Mosenfelder, 2000).

Three separate series of high-pressure diffraction measurements were performed on three different crystals, one from CS45 (denoted X1 here) and two from U1686 (X2 and X3). All three crystals were selected on the basis of optical quality, sharpness of their diffraction maxima, and the complete absence of the symmetry-violating reflections that would indicate the presence of (1 0 0) twins (Sasaki et al., 1983; Kirfel and Will, 1984). Each crystal was loaded into a BGI diamond-anvil pressure cell (Allan et al., 1996) with a 4:1 mixture of methanol and ethanol as the hydrostatic pressure medium and a quartz crystal for use as an internal pressure standard. A stishovite crystal was also loaded with crystal X2, which was therefore smaller

Table 1
Unit-cell parameters of coesite at high pressures[a]

	P (Gpa)	a (Å)	b (Å)	c (Å)	β (°)	V (Å^3)
X1P0	1×10^{-4}	7.1366 (2)	12.3723 (4)	7.1749 (3)	120.331 (2)	546.80 (3)
X1P1	0.547 (4)	7.1190 (3)	12.3553 (4)	7.1683 (3)	120.388 (2)	543.88 (3)
X1P8	2.248 (6)	7.0666 (3)	12.3049 (4)	7.1462 (3)	120.541 (2)	535.19 (3)
X1P2	2.375 (5)	7.0618 (2)	12.3001 (3)	7.1445 (2)	120.556 (1)	534.41 (3)
X1P3	3.763 (5)	7.0203 (2)	12.2615 (3)	7.1260 (3)	120.665 (1)	527.63 (3)
X1P4	5.164 (7)	6.9804 (2)	12.2255 (3)	7.1075 (3)	120.759 (1)	521.22 (3)
X1P5	6.509 (6)	6.9450 (2)	12.1909 (4)	7.0912 (3)	120.845 (2)	515.46 (3)
X1P6	7.655 (8)	6.9614 (2)	12.1644 (3)	7.0768 (3)	120.902 (3)	510.88 (3)
X1P7	7.814 (11)	6.9126 (3)	12.1610 (5)	7.0746 (3)	120.907 (2)	510.27 (3)
X2P0	1×10^{-4}	7.1356 (4)	12.3698 (6)	7.1729 (4)	120.330 (2)	546.47 (5)
X2P2	1.168 (6)	7.0984 (4)	12.3345 (9)	7.1586 (4)	120.445 (3)	540.35 (6)
X2P1	2.299 (8)	7.0635 (3)	12.3013 (5)	7.1437 (3)	120.547 (2)	534.57 (4)
X2P3	3.137 (8)	7.0384 (5)	12.2790 (10)	7.1328 (5)	120.614 (3)	530.53 (6)
X2P4	4.252 (8)	7.0050 (3)	12.2467 (6)	7.1179 (3)	120.694 (2)	525.08 (4)
X2P5	5.037 (11)	6.9833 (4)	12.2269 (7)	7.1077 (3)	120.750 (2)	521.56 (5)
X2P6	5.851 (9)	6.9614 (4)	12.2062 (9)	7.0977 (3)	120.796 (2)	518.06 (5)
X2P7	6.613 (8)	6.9418 (3)	12.1875 (8)	7.0877 (3)	120.846 (2)	514.82 (5)
X2P8	7.504 (9)	6.9191 (3)	12.1660 (5)	7.0766 (3)	120.891 (2)	511.19 (3)
X2P9	8.264 (11)	6.9016 (4)	12.1497 (7)	7.0681 (3)	120.928 (2)	508.41 (5)
X2P10	9.635 (12)	6.8704 (4)	12.1164 (7)	7.0520 (3)	120.986 (2)	503.27 (5)
X3P0	1×10^{-4}	7.13648 (11)	12.3716 (4)	7.1743 (4)	120.335 (1)	546.69 (2)
X3P2	0.642 (3)	7.11597 (15)	12.3516 (5)	7.16621 (16)	120.397 (1)	543.28 (3)
X3P1	1.363 (4)	7.09297 (12)	12.3292 (4)	7.15681 (13)	120.465 (1)	539.46 (3)
X3P4	1.941 (4)	7.07491 (13)	12.3121 (4)	7.14917 (14)	120.515 (1)	536.49 (3)
X3P3	2.539 (3)	7.05664 (11)	12.2945 (3)	7.14112 (13)	120.569 (1)	533.45 (2)
X3P12	3.564 (5)	7.02600 (10)	12.2665 (3)	7.12764 (12)	120.649 (1)	528.48 (2)
X3P5	4.137 (5)	7.00910 (3)	12.2510 (7)	7.1203 (3)	120.688 (2)	525.79 (4)
X3P10	4.900 (6)	6.98770 (11)	12.2307 (3)	7.11052 (13)	120.744 (1)	522.29 (2)
X3P6	6.210 (6)	6.95288 (12)	12.1975 (4)	7.09383 (14)	120.826 (1)	516.62 (3)
X3P11	7.123 (7)	6.92974 (13)	12.1753 (4)	7.0821 (4)	120.873 (1)	512.86 (3)
X3P7	8.392 (6)	6.89878 (10)	12.1461 (3)	7.06691 (13)	120.937 (1)	507.91 (2)
X3P8	9.162 (6)	6.88107 (11)	12.1287 (3)	7.05793 (13)	120.970 (1)	505.07 (2)
X3P9	9.689 (9)	6.86997 (18)	12.1184 (5)	7.0521 (2)	120.992 (2)	503.29 (4)

[a] Estimated standard deviations in the last decimal place of each value are given in parentheses.

than the other crystals and yielded larger uncertainties in the results. Unit-cell parameters of each crystal at each pressure were obtained by vector least-squares fit (Ralph and Finger, 1982) to the diffractometer setting angles of between 15 and 20 strong reflections determined by the SINGLE software (Angel et al., 2001) on a Huber four-circle diffractometer (Angel et al., 1997). The unit-cell volume of quartz was used to determine the pressure through its equation of state (Angel et al., 1997). Pressures and unit-cell parameters are listed in Table 1. The three sets of unit-cell data from the three crystals exhibit small but significant differences that arise from the use of different peak-centring algorithms on the diffractometer, but the trends with pressure are identical within the mutual uncertainties. In the following, we therefore discuss in detail the results obtained from the largest dataset (from X3) with the understanding that the other two datasets exhibit the same behaviour.

Up to the maximum pressures achieved in these experiments (~9.6 GPa) there are no discontinuities or changes in slope in either the unit-cell volume or the unit-cell parameters with pressure (Fig. 1). Neither were there any significant deviations from monoclinic lattice symmetry, any significant change in the intensities of the reflections, nor any increase

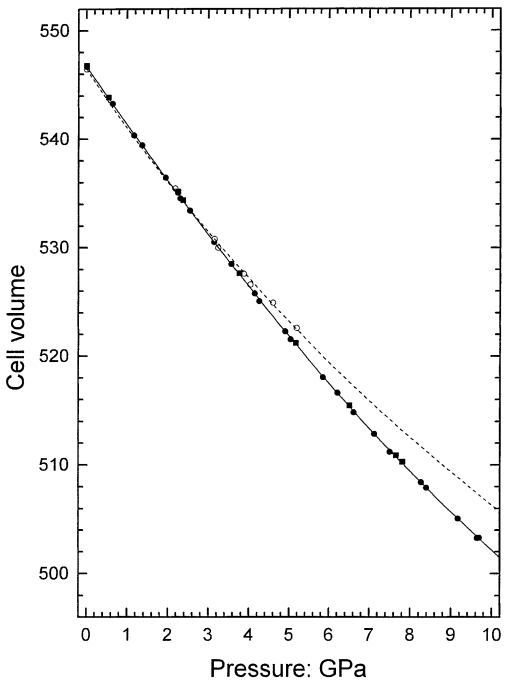

Fig. 1. Measured unit-cell volumes of coesite as a function of pressure. Solid symbols from this work, with the fourth-order Birch–Murnaghan fit to the data of crystal X3 shown as a solid line. The third-order EoS is indistinguishable on the scale of this figure. Open symbols and dashed line are from Levien and Prewitt (1981). Symbol sizes are approximately equivalent to ±10 esd's in unit-cell volumes and pressures.

in the widths of the diffraction peaks. We, therefore, conclude that coesite does not undergo any phase transitions at room temperature in this pressure regime, in agreement with previous experimental observations by diffraction (Levien and Prewitt, 1981) and spectroscopy (Hemley, 1987; Williams et al., 1993). Our data confirm the results of one recent computer simulation of the high-pressure behaviour of coesite (Gibbs et al., 2000) but not that of Dean et al. (2000) who predicted a phase transition at 8 GPa.

3. Equation of state

Equation of state parameters were obtained by fully-weighted least-squares refinements (Angel, 2001) to the *P–V* data sets. A third-order Birch–Murnaghan EoS fitted to the X3 dataset yields $K_{T0} = 97.4 \pm 0.6$ GPa and $K'_0 = 4.3 \pm 0.2$. This bulk modulus value is indistinguishable from the $K_{T0} = 96 \pm 3$ GPa obtained by Levien and Prewitt (1981) from single-crystal data to a maximum pressure of 5.2 GPa. Their value of $K'_0 = 8.4$ clearly arises from the divergence of their two highest-pressure data points to larger volumes, which is not consistent with the continuing smooth evolution of volume with pressure that we measured up to 9.6 GPa (Fig. 1).

However, the large value of $\chi^2_w = 8.1$ obtained for the fit of the BM3 Equation of State indicates that it does not fit the X3 data adequately. The same is also true for the Vinet, Murnaghan and third-order natural strain equations of state. All yield very similar values of K_{T0} (ranging from 97.3 to 97.5 GPa) and K'_0 (4.1–4.4) and large values of χ^2_w (ranging from 7.3 for a Murnaghan EoS to 9.1 for a third-order natural strain EoS). The reason for this misfit can be illustrated by re-formulating the Birch–Murnaghan EoS in terms of the Eulerian strain $f = [(V_0/V)^{2/3} - 1]/2$ and a normalised stress $F = P/3f(1+2f)^{5/2}$. To fourth-order in strain, the relationship is

$$F = K_{T0} + K_{T0}(K'_T - 4)f + K_{T0} \times \left[K_{T0}K'_0 + (K'_0 - 4)(K'_0 - 3) + \frac{35}{9}\right] f^2$$

Analogous relationships can be derived for the natural strain and Vinet EoS (e.g. Angel, 2001). If, as for most materials, the *P–V* data can be adequately described by a third-order truncation of the EoS, then the coefficient of f^2 is zero and the data would lie on a straight line in a plot of F against f with slope $K_{T0}(K'_0 - 4)$ and an intercept at $f = 0$ on the F-axis of $F = K_{T0}$. By contrast, the data of all three coesite crystals plot on curves (Fig. 2), clearly indicating that the coefficient of f^2 is non-zero. Therefore, the compression of coesite can only be described by an EoS of *at least* fourth-order. Fitting the *P–V* data for X3 with a fourth-order Birch–Murnaghan EoS results in a large and significant reduction of χ^2_w to 0.7, and parameters $K_{T0} = 100.8 \pm 0.5$ GPa, $K'_0 = 1.8 \pm 0.3$. The refined value of the second derivative of bulk modulus with respect to pressure, K''_0, is large and positive, $+0.57 \pm 0.06\,\text{GPa}^{-1}$. This is significantly different from the negative value of $K''_0 = [(4 - K'_0)(K'_0 - 3) - 35/9]/K_{0T} = -0.044\,\text{GPa}^{-1}$ implied by the third-order truncation of the EoS. The fourth-order

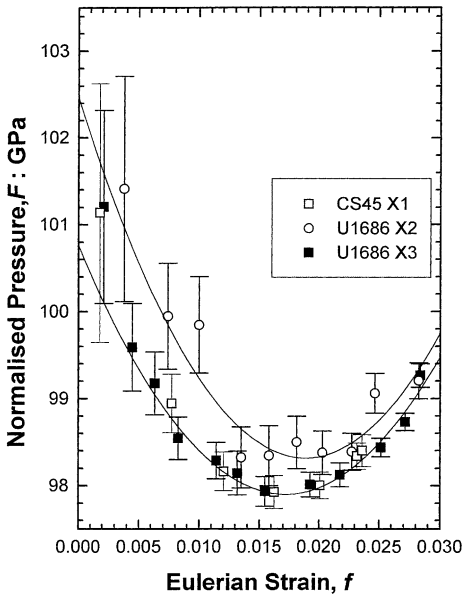

Fig. 2. Single-crystal compression data for all three measured crystals of coesite plotted as normalised pressure (F) against Eulerian strain (f). All three datasets show strong curvature, indicating that at least a fourth-order equation of state is necessary to fit the data. The two lines are fits to the data for X2 and X3. Error bars in f include the contributions from the uncertainties in P and V of each data point, as well as from the esd of V_0 (Angel, 2001). The offset of the X2 data arises from the slightly smaller value of V_0 of this crystal, but the overlap in the error bars of the X2 data with those of the other crystals indicates that offset of this dataset is only of the order of 1 esd in the experimental determinations.

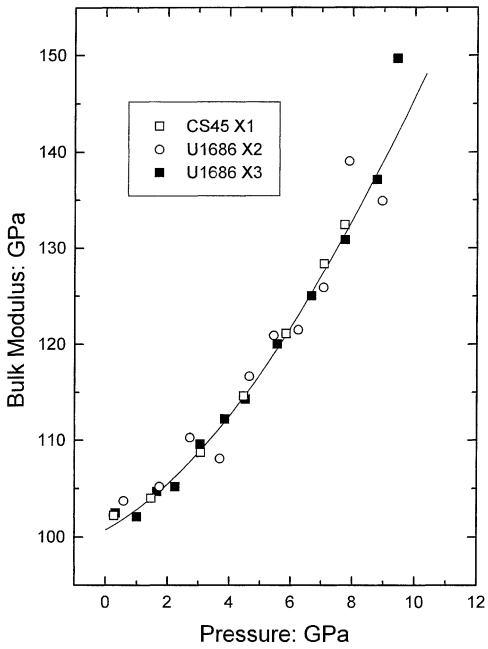

Fig. 3. Evolution of the bulk modulus of coesite with pressure. Points were calculated directly from consecutive pairs of P–V data as $K = (V_{i+1} + V_i)(P_{i+1} - P_i)/2(V_i - V_{i+1})$, plotted at the average pressure $(P_{i+1} + P_i)/2$. The line is bulk modulus predicted by the coefficients obtained from the fit of the fourth-order Birch–Murnaghan EoS to the P–V data of sample X3.

natural strain EoS yields indistinguishable values for the EoS parameters and the same quality of fit. Indistinguishable values are also obtained from fitting the data from X1. The fit to the X2 data provides a slightly higher value of $K_{0T} = 102.5 \pm 1.1$ GPa, and lower value of $K_0' = 1.1 \pm 0.6$. However, because of the strong negative correlation between these two parameters in the least-squares refinements the 95% confidence ellipses in K_{T0} and K_0' from the X1 and X3 refinements exhibit a large region of mutual overlap.

The second derivative of the bulk modulus, K_0'', normally has an implied negative value in a third-order EoS. This means that the rate at which most materials become stiffer decreases with increasing pressure. By contrast, the positive value of K_0'' for coesite indicates that it stiffens *more* rapidly as pressure increases, at least up to 10 GPa (Fig. 3). Note that at the highest pressures the value of the bulk modulus derived from the EoS parameters obtained from fitting the P–V data is smaller than that calculated directly from the P–V data. Similarly, linear extrapolation of the lowest pressure data on the f–F plot to $f = 0$ would suggest that the value of K_{T0} should be a little higher, around 102 GPa, than the value obtained from the fit of the BM4 EoS to the P–V data. Both of these observations indicate that the BM4 EoS does not fully describe high-pressure elasticity of coesite and that, in this respect as well as the positive value for K_0'', its compression behaviour can be termed anomalous.

4. Unit cell compression

Some further insights into the compressional behaviour of coesite can be obtained by examining the variation of the unit-cell parameters with pressure. Because coesite has monoclinic symmetry, one of the

Table 2
Elastic compliance matrix of coesite at room pressure and temperature[a]

ij	1	2	3	4	5	6
1	0.01094	−0.00321	−0.00263	0	−0.00346	0
2	−0.00321	0.00553	0.00015	0	0.00254	0
3	−0.00263	0.00015	0.00408	0	0.00151	0
4	0	0	0	0.01793	0	−0.00226
5	−0.00346	0.00254	0.00151	0	0.02117	0
6	0	0	0	−0.00226	0	0.01463

[a] Values in GPa^{-1} recalculated from Weidner and Carleton (1977) for a Cartesian co-ordinate system with $X_1||a^*$, $X_2||b$, $X_3||c$. In Table 2 of Weidner and Carleton (1977) the value of s_{22} is incorrectly given as $0.00533\,GPa^{-1}$.

principal axes of compression is constrained to lie along the diad axis (i.e. the *b*-axis), while the other two principal axes must lie in the (0 1 0) plane. Calculation of the strain ellipsoids from the data in Table 1 shows that they do not rotate significantly with pressure, and that the principal axes of compression lie within 2° of the (1 0 0) plane normal and the *c*-axis. Therefore, compression of $d(1\,0\,0) = a \sin\beta$, *b* and *c* are used in the following to completely describe the compression of the coesite unit cell. For this reason it is also convenient to transform the components of the elasticity tensors determined by Brillouin spectroscopy (Weidner and Carleton, 1977) to a Cartesian co-ordinate system with $X_1||a^*$, $X_2||b$, $X_3||c$. The resulting values of the components of the elastic compliance tensor, s_{ijkl}, are listed in matrix form in Table 2. Brillouin spectroscopy yields adiabatic elastic compliances s^{S}_{ijkl}, which should therefore be converted to isothermal values s^{T}_{ijkl} for comparison with data obtained from isothermal compression experiments. The relationship between the two compliance tensors is $s^{T}_{ijkl} = s^{S}_{ijkl} + \alpha_{ij}\alpha_{kl}(T/C_p)$ in which *T* is the temperature, C_p is the isobaric heat capacity, and α_{kl} is the thermal expansion tensor (Nye, 1957). Unit-cell parameter data for coesite have been measured as a function of temperature from 103 to 600 K (Galkin et al., 1987). Polynomial fits to these data can be used to derive (following Schlenker et al., 1975 and Pauffler and Weber, 1999) the components of the thermal expansion tensor of coesite (Table 3) at room temperature. When these values are combined with the heat capacity of $2.13 \times 10^6\,J\,m^{-3}\,K^{-1}$ (Hemingway et al., 1998) the adiabatic to isothermal correction terms are found to be of the order of $10^{-15}\,Pa^{-1}$, or <1 part in 10^4 of the values of the components s_{ijkl}. These corrections are deemed insignificant, and have therefore not been applied to the values given in Table 2.

Table 3
Thermal expansion tensor of coesite at 300 K and room pressure[a]

ij	1	2	3
1	4.45	0.	0.74
2	0	1.26	0
3	0.74	0	0.55

[a] Values in $10^{-6}\,K^{-1}$ recalculated from the unit-cell data Galkin et al. (1987) for a Cartesian co-ordinate system with $X_1||a^*$, $X_2||b$, $X_3||c$.

The *f–F* plots of the axial data (Fig. 4) indicate that the compression of the *b*-axis can be adequately described by a third-order EOS, whereas that of $d(1\,0\,0)$ and the *c*-axis require a fourth-order EOS. The parameters obtained from fitting these orders of the Birch–Murnaghan EoS to the cubes of the unit-cell parameters (Angel, 2001) are listed in Table 4. There is reasonable agreement between the room pressure moduli from these fits with those calculated from the elastic compliance tensor obtained from Brillouin measurements (Weidner and Carleton, 1977). The compression of coesite is extremely anisotropic, with the (1 0 0) plane normal being the softest direction. It is twice as soft as the *b*-axis, and three times as soft as the *c*-axis. In other terms, some 60% of the volume reduction under hydrostatic pressure is accommodated by the reduction in $d(1\,0\,0)$. The same anisotropy is displayed by the room temperature thermal expansion of coesite, with this same direction accounting for ∼70% of the total volume expansion (Table 3), and the *c*-axis showing the smallest variation with temperature.

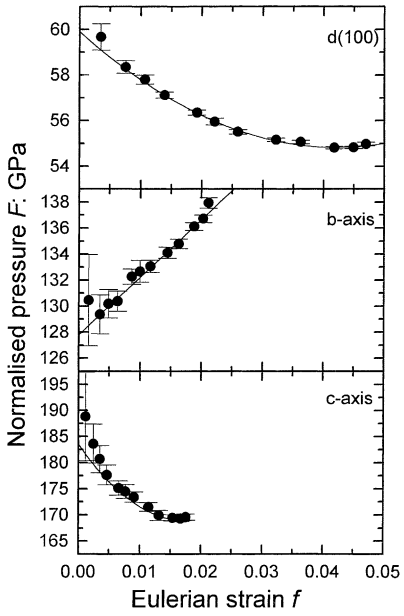

Fig. 4. The linear compression data for sample X3 along the principal axes of the compression ellipsoid (i.e. $d(1\,0\,0)$, b and c) plotted as normalised pressure (F) against Eulerian strain ($f = [(x_0/x)^2 - 1]/2$). Error bars in f include the contributions from the uncertainties in P and V of each data point, as well as from the zero-pressure cell parameters (Angel, 2001). The lines are the Birch–Murnaghan fits to the P–x data (Table 4). The curvature in the plots for $d(1\,0\,0)$ and the c-axis are visual indications that the data cannot be fitted with a third-order EoS. The data for the other two samples are omitted for clarity.

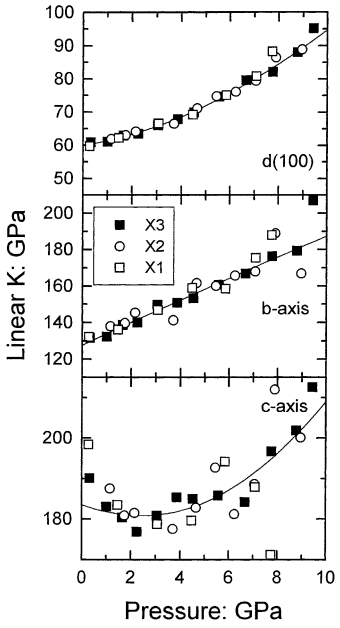

Fig. 5. Linear moduli for the principal axes of the compression ellipsoid (i.e. d$(1\,0\,0)$, b and c) of coesite. Points were calculated directly from consecutive pairs of P–x data as $K_x = (x_{i+1} + x_i)(P_{i+1} - P_i)/6(x_i - x_{i+1})$, plotted at the average pressure $(P_{i+1} + P_i)/2$. The lines are the moduli predicted by the coefficients obtained from the fit of the Birch–Murnaghan EoS to the P–x data of sample X3 (Table 4).

The compression data for $d(1\,0\,0)$ and b are well described by the EoS fits (Figs. 4 and 5), although there is a suggestion from Fig. 5 that the elasticity of the axes is not properly described at the highest pressures. But, as for the volume compression, closer examination of Fig. 4 shows that the BM4 equation underestimates the room-pressure compressional modulus of the c-axis. A linear fit to the lowest-pressure f–F data would suggest that K_{0c} should be about 192 GPa rather than the 184 ± 3 GPa obtained from a fit to all of the data. The same is suggested by the linear compression moduli calculated directly from pairs of consecutive P–c

Table 4
Parameters of axial compression of coesite, crystal X3[a]

	$X_1 \| a^*$	$X_2 \| b$	$X_3 \| c$
x_0 (Å)	6.15945 (10)	12.3717 (3)	7.17456 (19)
K_{T0} (Gpa)	59.9 (3)	127.8 (7)	184 (3)
K'_{T0}	1.31 (15)	6.31 (17)	−2.1 (1.1)
K''_{T0}(GPa^{-1})	0.39 (3)	[−0.090]	0.76 (15)
χ^2_w of fit	0.87	0.81	0.63
K_{0S} (GPa) (Weidner and Carleton, 1977)	65.4	135.0	208.3

[a] Numbers in parentheses are the esd's in the last decimal place of each value, obtained from the variance-covariance matrix of the least-squares fit. The number in the square bracket is the implied value of K_{0T} for the third-order EoS fit.

data points (Fig. 5). A value of ~192 GPa, while not consistent with the value of 208 GPa obtained from Brillouin measurements (Weidner and Carleton, 1977), is certainly closer. Fig. 5 also highlights the fact that the *c*-axis of coesite becomes slightly *softer* with increasing pressure from 0 to ~2.5 GPa, as also indicated by the *negative* value of K_0' for this axis (Table 4). As pressure increases, the positive value of K'' returns K' to a positive value and above ~2.5 GPa the linear modulus for the *c*-axis increases with pressure. The linear modulus of the *c*-axis under hydrostatic compression is given by summing elements of the elastic compliance matrix; $K_{0c} = (s_{13} + s_{23} + s_{33})^{-1}/3$. Normally the components of s decrease with increasing pressure, leading to an increase in linear moduli such as K_{0c}. In the case of the *c*-axis of coesite, our compressional data show that the sum $(s_{13} + s_{23} + s_{33})$ must increase upon initial compression. It seems unlikely that the pressure derivative of s_{33} would be positive, so we would suggest that at least one of the two shear moduli s_{13} and s_{23} has a positive pressure derivative.

5. Conclusions

At low pressures, below 3 GPa, the new EoS of coesite is indistinguishable from that measured by Levien and Prewitt (1981). Therefore, there are no significant differences in the calculated volume or impedence change associated with the quartz-coesite transition. However, the new direct measurements of the compression of coesite to 9.6 GPa show that it is approximately 1% denser at 9–10 GPa (at room temperature) than predicted by extrapolation of the EoS obtained by Levien and Prewitt (1981). The resulting shift in the calculated position of the equilibrium coesite-stishovite phase boundary is small, of the order of 0.05 GPa, because the ΔV of the transition is so large. But, at pressures in excess of 8 GPa, the bulk modulus of coesite is some 20 GPa less than that previously predicted, and the impedence constrast between coesite and stishovite is therefore some 10% greater than would have been estimated on the basis of the previous EoS parameters.

It should be noted that for the purposes of obtaining the volume of coesite at high pressures for use in, for example, thermodynamic calculations, our third-order Birch–Murnaghan EoS with $K_{T0} = 97.4$ GPa and $K = 4.3$ is probably sufficiently accurate. At pressures up to 10 GPa it yields volumes for coesite that deviate by <0.05% from those given by the fourth-order EoS. However, the elasticity of coesite is not adequately represented by a third-order EoS because this requires the second pressure derivative K_0'' of the bulk modulus to be negative, whereas the data (Fig. 2) show that of coesite is significantly positive. This means that the rate at which coesite becomes stiffer with increasing pressure *increases* rather than decreases with increasing pressure (Fig. 3). A simple-minded explanation of this result is that coesite, as a structure only stable at high pressures, is over-expanded at room pressure. Initial rapid compression would then occur until a pressure >3.5 GPa at which point, with the structure compressed to a more "normal" configuration of Si–O–Si bonds, the compressional behaviour also becomes more "normal" with a slightly positive slope in the *f–F* plot (Fig. 3). This anomalous evolution of the volume and bulk modulus appears to have its cause in the anomalous behaviour of the *c*-axis which becomes softer upon initial compression up to ~2.5 GPa. We have no explanation for this unusual observation, except that it might be related to the unusual positive value for the elastic compliance matrix element s_{23} at room pressure. This means that initial compression of the *b*-axis contributes to a *contraction*, rather than an expansion, of the *c*-axis (and *vice-versa*). Further understanding of this behaviour must await the measurement of the elastic moduli of coesite in situ at high pressures and a determination of the evolution of the structure of coesite to higher pressures than the currently available data (Levien and Prewitt, 1981).

The identification of this anomalous behaviour partially resolves the discrepancy between the values of the bulk moduli of coesite obtained by Brillouin scattering (Weidner and Carleton, 1977) and isothermal compression which was partly due to two errant data points at the highest pressures achieved by Levien and Prewitt (1981). Nonetheless, our preferred value of $K_{0T} = 100.8 \pm 0.5$ GPa from the fourth-order Birch–Murnaghan EoS is still significantly less than the 109 GPa obtained from Brillouin spectroscopy (Weidner and Carleton, 1977), even allowing for an estimated uncertainty in the latter of the order of ±5.5 GPa which can be derived by propagation of the reported velocity misfits of ~0.15 km s^{-1}.

Acknowledgements

We would like to thank P.I. Dorogokupets, R.J. Hemley, P.J. O'Brien for helpful comments and discussions.

References

Allan, D.R., Miletich, R., Angel, R.J., 1996. A diamond-anvil cell for single-crystal X-ray diffraction studies to pressures in excess of 10 GPa. Rev. Sci. Instrum. 67, 840–842.

Angel, R.J., 1996. Bulk moduli of plagioclase feldspars, EoS Trans. AGU 77, F673.

Angel, R.J., 2001. Equations of state. In: Hazen, R.M., Downs, R.T. (Eds.), High-Pressure, High-Temperature Crystal Chemistry. Reviews in Mineralogy and Geochemistry, 41, in press.

Angel, R.J., Allan, D.R., Miletich, R., Finger, L.W., 1997. The use of quartz as an internal pressure standard in high-pressure crystallography. J. Appl. Crystallogr. 30, 461–466.

Angel, R.J., Downs, R.T., Finger, L.W., 2001. High-pressure, high-temperature diffractometry. In: Hazen, R.M., Downs, R.T. (Eds.), High-Pressure, High-Temperature Crystal Chemistry. Reviews in Mineralogy and Geochemistry, 41, in press.

Chopin, C., 1983. High-pressure facies series in pelitic rocks: a review. Terra Cognita 3, 183.

Dean, D.W., Wentzcovitch, R.M., Keskar, N., Chelikowsky, R., 2000. Pressure-induced amorphisation in crystalline silica: soft phonon modes and shear instabilities in coesite. Phys. Rev. B 61, 3303–3309.

Downs, R.T., Hazen, R.M., Finger, L.W., 1994. The high-pressure crystal chemistry of low albite and the origin of the pressure dependency of Al–Si ordering. Am. Mineral. 79, 1042–1052.

Galkin, V.M., Doroshev, A.M., Babich, Yu.V., 1987. The thermal expansion of coesite. Geokhimiya part 11, 1645–1646 (in Russian).

Gillet, P., Ingrin, J., Chopin, C., 1984. Coesite in subducted continental crust: *P–T* history from an elastic model. Earth Planet. Sci. Lett. 70, 426–436.

Hemingway, B.S., Bohlen, S.R., Hankins, W.B., Westrum, E.F., Kuskov, O.L., 1998. Heat capacity and thermodynamic properties for coesite and jadeite, re-examination of the quartz-coesite equilibrium boundary. Am. Mineral. 83, 409–418.

Hemley, R.J., 1987. Pressure dependence of Raman spectra of SiO_2 polymorphs: α-quartz, coesite, and stishovite. In: Manghnani, M.H., Syono, Y. (Eds.), High-Pressure Research in Mineral Physics. Terra Scientific Publishing Co., Tokyo, pp. 347–359.

Levien, L., Prewitt, C.T., 1981. High-pressure crystal structure and compressibility of coesite. Am. Mineral. 66, 324–333.

Kirfel, A., Will, G., 1984. Ending the "$P2_1/a$ coesite" discussion. Zeit. Kristallogr. 167, 287–291.

Mosenfelder, J.L., 2000. Pressure dependence of hydroxyl solubility in coesite. Phys. Chem. Miner. 27, 610–617.

Nye, J.F., 1957 Physical Properties of Crystals. Oxford University Press, Oxford, 329 pp.

Parkinson, C.D., 2000. Coesite inclusions and prograde compositional zonation of garnet in whiteschist of the HP-UHPM Kokchetav massif, Kazakhstan; a record of progressive UHP metamorphism. Lithos 52, 215–233.

Parkinson, C.D., Katayama, I., 1999. Present-day ultrahigh-pressure conditions of coesite inclusions in zircon and garnet: evidence from laser Raman microspectroscopy. Geology 27, 979–982.

Pauffler, P., Weber, T., 1999. On the determination of linear thermal expansion coefficients of triclinic crystals using X-ray diffraction. Eur. J. Miner. 11, 721–730.

Ralph, R.J., Finger, L.W., 1982. A computer program for refinement of crystal orientation matrix and lattice constants from diffractometer data with lattice symmetry constraints. J. Appl. Crystallogr. 15, 537–539.

Sasaki, S., Chen, H.-K., Prewitt, C.T., Nakajima, Y., 1983. Re-examination of "$P2_1/a$ coesite". Zeit. Kristallogr. 164, 67–77.

Schlenker, J.L., Gibbs, G.V., Boisen, M.B., 1975. Thermal expansion coefficients for monoclinic crystals: a phenomenological approach. Am. Miner. 60, 828–833.

Shaw, C.S.J., 1999. Dissolution of orthopyroxene in basanitic magma between 0.4 and 2 GPa: further implications for the origin of Si-rich alkaline glass inclusions in mantle xenoliths. Contrib. Miner. Petrol. 135, 114–132.

van der Molen, I., van Roermond, H.L.M., 1986. The pressure path of solid inclusions in minerals: the retention of coesite inclusions during uplift. Lithos 19, 317–324.

Weidner, D.J., Carleton, H.R., 1977. Elasticity of coesite. J. Geophy. Res. 82, 1334–1346.

Williams, Q., Revanaugh, J.S., 2000. The "X" discontinuity: a signature of deep fluid flow and free silica in the sub-continental mantle. EoS 81, F922.

Williams, Q., Hemley, R.J., Kruger, M.B., Jeanloz, R., 1993. High-pressure infra-red spectra of α-quartz, coesite, stishovite and silica glass. J. Geophy. Res. B 98, 22157–22170.

Woodland, A.B., Angel, R.J., 1997. Reversal of the orthoferrosilite — high-*P* clinoferrosilite transition, a phase diagram for $FeSiO_3$ and implications for the mineralogy of the earth's upper mantle. Eur. J. Miner. 9, 245–254.